**Proceedings of the ASME 2022**
**Internal Combustion Engine Division ICE Forward Conference**
**ICEF 2022**
**October 16-19, 2022, Indianapolis, Indiana, USA**

# ICEF2022-89674

# PARAMETRIC STUDIES OF DEFLAGRATION-TO-DETONATION TRANSITION IN A PRE-CHAMBER/MAIN-CHAMBER SYSTEM

**R. Zhu** [*], **X. Fang, M. Davy**
Department of Engineering Science
University of Oxford
Oxford, United Kingdom

**S. Tang***, **S. Lai** [†]
School of Aeronautics and Astronautics
Shanghai Jiao Tong University
Shanghai, China

**C. Xu**
Energy Systems Division
Argonne National Laboratory
Lemont, IL

## ABSTRACT

Numerical simulations are performed to study the process of flame propagation through a small orifice and transition to detonation in a confined pre-chamber/main-chamber system. The numerical model solves the fully compressible Navier-Stokes equations by a high-order numerical algorithm on a dynamically adapting mesh, coupled with a single-step chemical-diffusive model for a stoichiometric ethylene-oxygen mixture. Four successive stages, namely laminar flame propagation, jet flame formation, flame distortion by shock waves, and transition to detonation, are observed. Parametric studies with varying nozzle diameters and initial temperatures are tested to investigate the effect of nozzle size and the stochasticity of deflagration-to-detonation transition (DDT). The results suggest that the case with a smaller nozzle size, $d =$ 1.5 mm, requires a longer time for the flame to evolve and transition into a detonation. A small change in the initial temperature results in clear fluctuations of flame surface length in the turbulent flame regime. In addition, the case with the smaller orifice size is shown to be more sensitive to the initial temperature. Due to the stochastic nature of DDT, the time and location for detonation initiation vary in all cases. Nevertheless, the detonation mechanism remains the same and is independent of the small variations in the initial temperature or the orifice size.

[*]These authors contribute equally to the work
[†]Address all correspondence to this author.

## 1 Introduction

To comply with the stringent legislation on greenhouse gas and pollutant emissions, lean-burn engines, offering inherent advantages of high efficiency and low emissions, are being developed worldwide [1]. However, the practical exploitation of lean-burn combustion technology will require solutions to the known problems of lean mixtures such as low ignitability and misfire. Pre-chamber ignition systems have been proposed as an alternative to spark ignition due to the ability to sustain stable combustion of very lean mixtures [2]. To enable a wider range of lean operations, hot gas produced in the pre-chamber propagates into the main chamber through one or more orifices, forming turbulent reacting jet(s), and providing favorable local mixing and rapid combustion. As high-speed jet flames accelerate into the main chamber they can be accompanied by the generation of shock waves [3]. Under extreme conditions, deflagration-to-detonation transition (DDT) might occur in the main chamber, which is closely related to the "super knock" phenomenon [4]. While a number of studies have focused on the behaviour of super knock in research engines, no consensus has been reached on the exact mechanism of a super knock event. In fact, it is not clear whether there exists a single mechanism that can explain all super knock events. Nevertheless, studies have suggested that super knocks in SI engines may be driven by end-gas autoignition and flame/shock interactions [5]. Therefore, it is of great interest to numerically study the fundamentals of flame-shock interactions in pre-chamber/main-chamber systems with a particular focus on

DDT.

There have been a number of recent studies focusing on the effects of pre-chamber ignition and turbulent jet flame on main-chamber combustion [6–8], and the onset of DDT [4, 9] in real engines or combustion chambers under engine relevant conditions. Qin *et al.* [6] used direct numerical simulations to study the transient mixing and ignition mechanism of methane/air mixtures in a simplified pre-chamber/main-chamber system. It was shown that the mean burning velocity in the main chamber could be significantly elevated as the pre-chamber jet entered the main chamber. Recently, Wei and co-workers [4, 9, 10] carried out a series of experiments in a confined combustion chamber to study: the flame acceleration after passing through a perforated plate, the subsequent propagation of turbulent jet flame and shock waves, resultant end-gas autoignition, and the stochasticity of detonation initiation. They observed various combustion modes, including normal combustion, oscillating combustion, and end-gas autoignition with and without DDT near the end wall of the combustion chamber by adjusting the jet flame speed, initial pressure, and fuel/air equivalence ratio. It was concluded that the occurrence of DDT is closely related to turbulent characteristics of the jet flame and the later flame-shock interactions. In particular, the propensity of end-gas autoignition with developing detonation was found to be positively related to the main flame propagation velocity. While the combustion chamber provides physical insights for the study of super knock and DDT, the detailed mechanism of DDT was not revealed due to challenging experimental conditions.

DDT in pre-chamber/main-chamber systems or enclosed space, to the best of the authors' knowledge, is not well studied and understood. Some experimental and numerical studies focusing on DDT in open channels, however, can provide insights into the mechanism of DDT. Previous studies have suggested DDT initiation can be mainly attributed to two mechanisms 1) a delayed transition to detonation through a gradient of reactivity in the unburned gas by focusing of relatively weak shocks, and 2) direct detonation initiation by shock focusing and collision at the flame front [11, 12]. The DDT mechanism highlighted by Gamezo *et al.* [13] in a 2-D obstructed open channel containing a stoichiometric hydrogen-air mixture was found to be consistent with the first mechanism through the generation of explosive hot spots in the unburned gas. It was found that the explosive kernel in the unburned gas was induced through the Zel'dovich reactivity mechanism due to localised temperature or species gradients. Using the same numerical method, Xiao *et al.* [11] observed a hot spot induced by shock focusing with an idealized model. The hot spot later developed into a detonation via the first DDT initiation mechanism. From the same study, they also observed the onset of a direct detonation initiation spot at the flame front collided by shocks in a 2D obstructed channel, in accordance with the second DDT mechanism. Liberman *et al.* [14] experimentally and numerically observed detonation initiation at the vicinity of fast travelling flame brush in channels with no-slip walls. While the above-mentioned studies detailed the DDT initiation mechanisms in open channels, the flow and thermodynamic conditions in a closed-vessel could be significantly different as pressure builds up dramatically.

Researchers have highlighted the importance of studying the sensitivity of DDT to initial conditions as it can be critical for avoiding detrimental physical processes such as super knock. DDT in an obstructed channel has been shown to be a spatially and temporally stochastic process with minimal fluctuations of initial conditions [15, 16]. The stochasticity of DDT was found to rise from the complexity of a series of underlying stochastic physical phenomena, including turbulence, flow instabilities, flame-shock-vortex interactions, and the resulting hot spot formation. Naturally, detonation initiation in DDT is stochastic as it is typically triggered by one of several stochastic hot spots in a system [16]. The stochastic nature of DDT in a confined combustion chamber has been experimentally observed even with great efforts to maintain the same experimental conditions [4]. However, the experimental study was not able to confirm whether the mechanism of DDT initiation in a confined space can be used to explain the stochastic nature of DDT phenomena. Previous simulations have suggested that some systems are more susceptible to the stochastic behaviour of DDT than others, depending on their geometries and initial conditions [16]. Therefore, an improved understanding of the stochasticity of DDT in a pre-chamber/main-chamber system could be of great interest for the development of lean-burn engines.

This study aims to numerically investigate DDT phenomena in a pre-chamber/main-chamber system, with a particular interest in understanding the stochastic occurrence of DDT in a confined space. Detailed processes of pre-chamber ignition, jet flame generation, main-chamber flame development, and end-gas DDT will be discussed. Parametric studies are first conducted by varying the size of the orifice connecting the pre-chamber and the main chamber to investigate the geometric effect on DDT. The stochastic behaviour of DDT and the robustness of the detonation initiation mechanism is then evaluated using additional parametric study where the initial background temperature is varied slightly.

## 2 Physical and Numerical Setup

### 2.1 Physical Models

To simulate the physics of the high-speed reactive flow, the full set of Navier-Stokes equations for fully compressible and chemically reactive gas, is solved in this study. Here, we consider four governing equations, the conservation of mass, momentum, energy, and species:

$$\frac{\partial \rho}{\partial t} + \nabla \cdot (\rho \mathbf{U}) = 0, \tag{1}$$

$$\frac{\partial (\rho \mathbf{U})}{\partial t} + \nabla \cdot (\rho \mathbf{U}\mathbf{U}) + \nabla p = \nabla \cdot \hat{\tau}, \tag{2}$$

$$\frac{\partial (\rho E)}{\partial t} + \nabla \cdot ((\rho E + p)\mathbf{U}) = \nabla \cdot (\mathbf{U} \cdot \hat{\tau}) + \nabla \cdot (K \nabla T) - \rho q \dot{\omega}, \tag{3}$$

$$\frac{\partial (\rho Y)}{\partial t} + \nabla \cdot (\rho Y \mathbf{U}) = \nabla \cdot (\rho D \nabla Y) + \rho \dot{\omega}, \tag{4}$$

where $\rho$, $T$, $p$, and $\mathbf{U}$ represent the density, temperature, pressure, and velocity of the gas. $E$ is the specific total energy, $\dot{\omega}$ is the chemical reaction rate, $q$ is the chemical energy release, $Y$ is the mass fraction of the reactant, $K$ is the thermal conductivity, and $D$ is the mass diffusivity.

The gas is assumed to obey the ideal gas equation of state,

$$p = \frac{\rho R T}{M}, \tag{5}$$

where $R$ is the universal gas constant, and $M$ is the molecular weight.

The viscous stress tensor is defined as

$$\hat{\tau} = \rho \nu ((\nabla \mathbf{U}) + (\nabla \mathbf{U})^T - \frac{2}{3}(\nabla \cdot \mathbf{U})\mathbf{I}), \tag{6}$$

where $\nu$ is the kinematic viscosity, $\mathbf{I}$ is the unit tensor, and the superscript $T$ stands for the matrix transposition.

The specific total energy $E$ is calculated by

$$E = \frac{p}{(\gamma - 1)\rho} + \frac{1}{2}(\mathbf{U} \cdot \mathbf{U}), \tag{7}$$

where $\gamma$ is the specific heat ratio.

A calibrated, one-step, chemical-diffusive model (CDM) [17] is used to study the premixed stoichiometric ethylene-oxygen combustion. The premixed combustion in the stoichiometric ethylene-oxygen mixture follows the single elementary reaction: C2H4 + 3O2 –> 2CO2 + 2H2O. The reaction follows a first-order Arrhenius equation, and the reaction rate is defined as

$$\dot{\omega} = \mathrm{d}Y/\mathrm{d}t = -A\rho Y \exp(-E_a/RT), \tag{8}$$

where $A$ represents the pre-exponential factor and $E_a$ represents the activation energy. The input parameters shown in Table 1 are carefully calibrated to reproduce the correct flame and detonation properties of the stoichiometric ethylene-oxygen mixture at one atmosphere. The simplified chemistry model approach used in this study has been extensively tested and used to solve various combustion problems including laminar flame propagation, flame-shock interactions, and DDT [18].

**TABLE 1**: Input model parameters and output combustion wave properties for stoichiometric premixed ethylene and oxygen initially at 1 atm and 298 K

| Parameter | Descriptions | Value |
|---|---|---|
| | **Input** | |
| $T_0$ | Initial temperature | 298 K |
| $P_0$ | Initial pressure | 1 atm |
| $\rho_0$ | Initial density | $1.27\times10^{-3}$ g/cm$^3$ |
| $\gamma$ | Adiabatic index | 1.2195 |
| $M$ | Molecular weight | 31 g/mol |
| $A$ | Pre-exponential factor | $1.05\times10^{12}$ cm$^3$/(g-s) |
| $E_a$ | Activation energy | 39.2 $RT_0$ |
| $q$ | Chemical energy release | 59.7 $RT_0/M$ |
| $\nu_0$ | Viscosity | $7.0\times10^{-6}$ g/s-cm-K$^{0.7}$ |
| $\kappa_0 = D_0$ | Transport constants | $1.0\times10^{-5}$ g/s-cm-K$^{0.7}$ |
| | **Output** | |
| $S_\mathrm{L}$ | Laminar flame speed | 413 cm/s |
| $T_\mathrm{b}$ | Post-flame temperature | $11.7T_0$ |
| $\rho_\mathrm{b}$ | Post-flame density | $0.085\rho_0$ |
| $\chi_\mathrm{l}$ | Laminar flame thickness | $8.88\times10^{-3}$ cm |

## 2.2 Numerical Models

The governing equations are solved using a fifth-order WENO algorithm with HLLC fluxes [19]. The time integration is advanced by a 3rd-order Runge-Kutta scheme [20]. The WENO method used in this study is a type of monotone-integrated large eddy simulation (MILES) algorithm. The MILES method can model turbulent dissipation at the sub-grid scale by the numerical dissipation inherent to the algorithm and does not require an additional explicit filter for

the sub-grid scale. A number of previous studies investigating turbulent, high-speed, reacting flows have shown that simulation results using MILES agree both qualitatively and quantitatively with experiments [21–24]. An adaptive mesh refinement (AMR) technique through the Boxlib library [25] is used to provide additional resolution near shocks and flames. The numerical simulation uses a minimum cell size of $dx_{min}$ = 26.0 $\mu$m. The choice of grid size takes into account both computational efficiency and accuracy.

### 2.3 Computational Details

Figure 1 shows the geometric configuration of the combustion chamber being investigated. Motivated by the pre-chamber ignition study of [8], the two-dimensional domain consists of the left pre-chamber with the dimension of 6 cm $\times$ 2.6 cm, and the main-chamber with the dimension of 7 cm $\times$ 10 cm. The two chambers are connected using an orifice with varying diameters. Non-slip, adiabatic boundaries are applied to all chamber walls. To ignite the mixture, a region of hot, burned product with a radius of 1 cm at 1500 K is placed at the left of the pre-chamber.

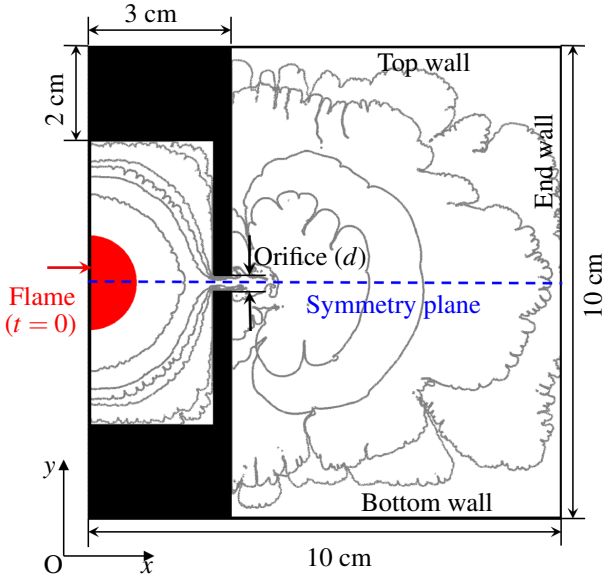


**FIGURE 1**: Computation domain of the pre-chamber/main-chamber system connected via an orifice. No-slip, reflecting, and adiabatic boundaries are used for all walls. The solid curves indicate a sequence of flame surface locations (the flame front is defined as $Y$=0.5).

## 3 Results and Discussion

### 3.1 Flame Acceleration and DDT

The overall process of flame acceleration and transition to detonation in the closed chamber is shown in Fig. 2 (a) $\sim$ (d). There are four stages in the simulation shown: (1) laminar flame propagation in the pre-chamber, (2) formation of the jet flame, (3) flame distortion in the main chamber by shock-flame interactions, and (4) a detonation initiation by shock-focusing mechanism. These stages are common for this configuration with different nozzle diameters, and therefore we provide some detailed descriptions for a certain case in the following paragraphs.

The process of laminar flame propagation in the left chamber is shown in Fig. 2(a). As the flame propagates, a series of pressure waves are induced in front of the flame (42.8 $\mu$s in Fig. 2(a)). As the pressure waves reach the orifice, they bounce back from the wall, forming a series of reflected pressure waves. The reflected pressure waves again hit the propagating flame front, producing complicated interlaced patterns (150.6 $\mu$s in Fig. 2(a)). In addition, the interactions between the reflected pressure waves and the flame front produce some small instabilities on the flame front. These instabilities remain relatively small, and the process of flame propagation can be regarded as a laminar flame expansion. At this stage, the flame speed and the flame surface area increase slowly.

As the flame propagates through the orifice, a jet flame structure is formed. Fig. 2(b) shows a series of velocity magnitude (top) and schlieren (bottom) fields illustrating the jet flame formation in the main chamber. As the jet flame forms, pressure waves are generated in front of the flame tip, forming a strong leading shock wave (indicated in Fig.2(b)). The burned mixture passing through the orifice pushes the gas ahead at high speed, producing strong vorticity near the orifice. The vorticity promotes the turbulent flame development and leads to a rapid increase of flame surface area (354.1 $\mu$s). At 412.9 $\mu$s, as the flame moves further away from the orifice, the intensity of vorticity is reduced, and the flame structure becomes less wrinkled.

The next stage, namely the "flame distortion by shock-flame interactions", is crucial for the turbulent flame development and the eventual detonation transition. Fig. 2(c) shows a series of schlieren fields illustrating this process. At 501.5 $\mu$s, the primary shocks hit the chamber wall and bounce back, forming reflected shock waves. The reflected shocks then propagate into the flame, producing a transmitted shock and another reflected shock wave (546.6 $\mu$s in Fig. 2(c)). This shock-flame interaction induces some fluid instabilities on the flame surface. These instabilities soon develop into large winkles, making the flame structure more turbulent. As the flame propagates, the repeated shock-flame interactions continuously distort the flame front, forming finger flame structures at 621.5 $\mu$s.

The flame is continuously distorted by the pressure waves and reflected waves, and eventually, a detonation spot is observed (marked in Fig. 2(d)). The right figures enlarge the region around the detonation spot just before and after the detonation is initiated. Here, two shocks (marked as "Shock 1"

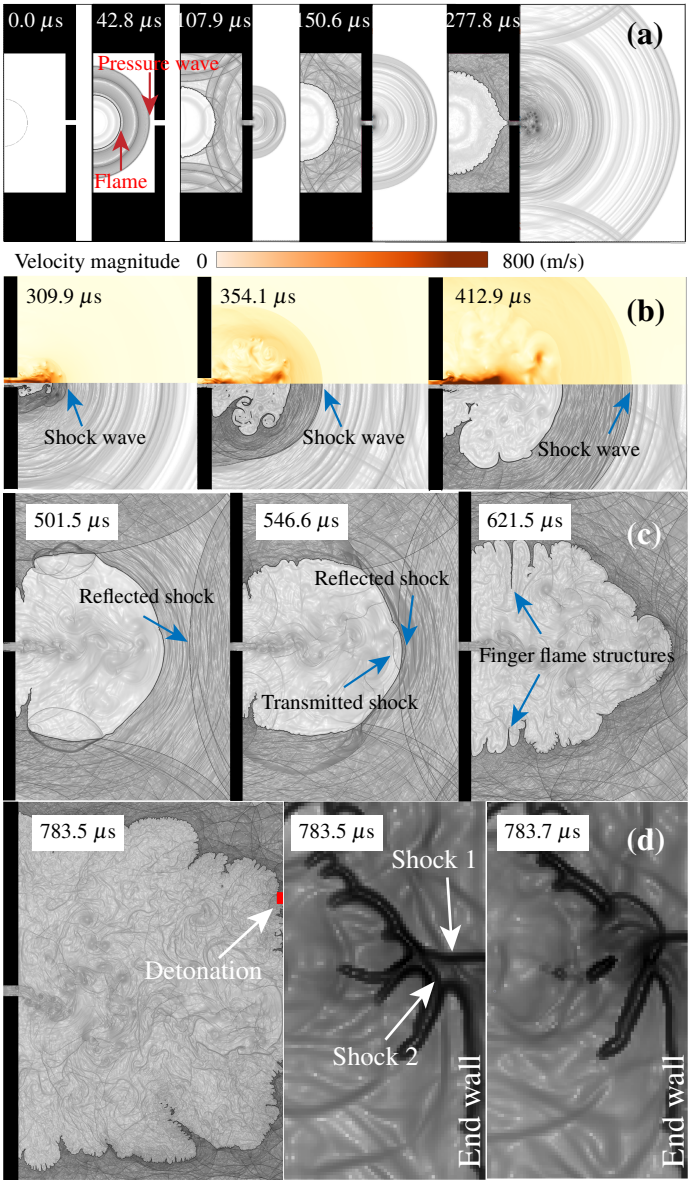


**FIGURE 2**: Sequence of (a) schlieren fields of laminar flame propagation in the pre-chamber; (b) Top: velocity magnitudes; Bottom: schlieren fields of hot jet formation at three different times; (c) schlieren fields of turbulent flame development in the main-chamber; (d) original and enlarged schlieren fields showing detonation. The time in microseconds is shown in the top left corners of the frames.

and "Shock 2") collide with each other at the flame front, causing an auto-ignition at 783.7 $\mu$s. In this study, the detonations always arise due to this shock-focusing mechanism (see more in Section 3.2.3).

## 3.2 Parametric Studies of System Configuration and Stochasticity

### 3.2.1 Effects of Orifice Size

Based on the experimental work done by Wei *et al.* [3], the size of the orifice is an important parameter affecting the speed of the jet flame and may eventually influence the overall flame propagation and detonation process. To investigate the effect of orifice size, the pre-chamber/main-chamber systems with orifice sizes ($d$) of 3 mm and 1.5 mm are tested at an initial temperature ($T_0$) of 298 K. Each frame in Fig. 3 shows half of the main chamber (the upper half-section for $d = 3$ mm and the bottom half-section for $d = 1.5$ mm). The schlieren images shown for the two configurations are selected such that the flame front in both cases has reached a similar location.

From the first frame of Fig. 3, vortices are shown to be generated as the flame passes through both orifices. However, for the same flame travel distance, the jet flame with $d = 1.5$ mm is seen to take longer to develop compared to that with $d = 3$ mm. This is consistent with the findings from Zhou *et al.* [26] where they also suggested under the same conditions in a combustion bomb that higher initial jet flame propagation is observed with bigger orifice holes. This is likely attributed to the less restriction of the larger orifice on jet flame, enabling a stronger and more reactive jet to penetrate into the main chamber. The flame propagation after the larger orifice size is also seen to produce turbulent vortices with a larger eddy structure prior to the interactions with the reflected shock. In the following frames, where the turbulent flame begins to develop due to shock-flame interactions, followed by the formation of finger-like flames, and eventually, the onset of a detonation, the case with $d = 1.5$ mm is qualitatively similar to what is observed with $d = 3$ mm. However, there is an obvious delay for the case with $d = 1.5$ mm in terms of the flame propagation and detonation initiation process. The delay can be related to the experimental findings from Zhou *et al.* [10] where the propensity of end-gas autoignition with developing detonation is found to be positively related to the initial main flame propagation and oxygen concentration in gasoline-air mixtures. For the simulations covered in this work, though, both cases eventually develop into detonation due to the highly reactive nature of ethylene and the use of pure oxygen as the oxidizer.

A more quantitative description of the effects of the orifice size can be found in Fig. 4, where time histories of flame surface length are shown for both cases. The flame surface length gradually increases until around 0.29 ms for $d = 3$ mm and 0.32 ms for $d = 1.5$ mm as the laminar flame expands in the pre-chamber. Afterward, significant differences in the flame surface variations between the two cases are observed as the flame starts to go through the orifice and forms a highly turbulent jet flame in the main chamber; meanwhile, the flame surface grows dramatically from 0.29 to 0.35 ms for $d = 3$ mm

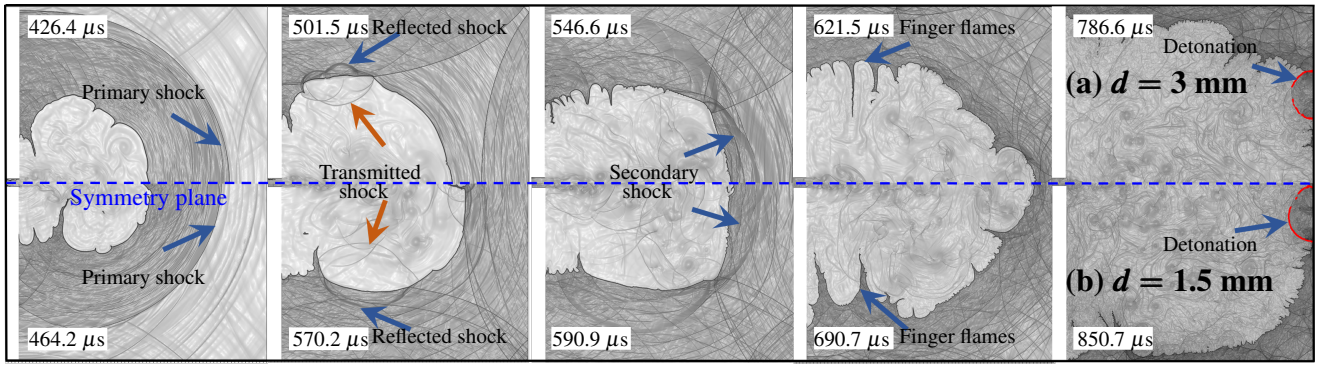


**FIGURE 3**: Sequence of schlieren fields when (a) $d = 3$ mm (top half ),and (b) $d = 1.5$ mm (bottom half) showing jet flame propagation, shock-flame interaction and onset of detonations (marked as Detonation). The blue dashed line indicates the symmetry plane.

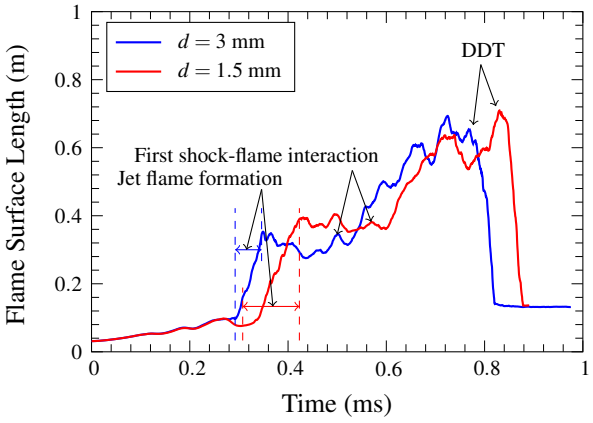


**FIGURE 4**: Time histories of computed flame surface length for orifice size $d = 3$ mm (blue) and 1.5 mm (red) when $T_0 = 298$ K.

and from 0.32 to 0.43 ms for $d = 1.5$ mm, i.e., marked as "Jet flame formation" in Fig. 4. It is clear from the time histories that the turbulent jet flame with a larger orifice size takes a shorter period before it spreads out in the main chamber, with the flame surface being less wrinkled as the interior vortices dissipate. This corresponds well with the schlieren field given by Fig. 3. Starting at 0.50 ms for $d = 3$ mm and 0.57 ms for $d = 1.5$ mm, i.e., marked as "First shock-flame interaction", the jet flame expands due to the perturbations induced by repeated shock-flame interactions. The flame surface is significantly increased with $d = 3$ mm and accelerated after the shock wave passed by arising from the Richtmyer–Meshkov (R–M) instabilities. Eventually, detonation occurs where the flame surface area drops rapidly as the detonation waves consume the unburned gas in the chamber, where the onset of DDT is found earlier with a larger orifice as highlighted before.

### 3.2.2 Stochastic Behaviours of DDT

Stochasticity can be defined as the ability of a process to deviate randomly from its mean path, where some systems can be more susceptible to stochastic behaviour than others depending on geometry, and initial conditions [18]. The stochasticity of DDT in the pre-chamber/main-chamber system is studied by varying initial temperatures of the mixture by small intervals (0.005 K or 0.01 K) for both $d = 3$ mm and $d = 1.5$ mm. The proposed method is adopted from Gamezo *et al.* [15]'s study on the stochastic dispersion for DDT in an obstructed open channel, where the proposed initial temperature fluctuations are considered too small to have systematic effects on the solution, but large enough to change the solution in a stochastic way. Fig. 5 shows schlieren field distributions of the main chamber (shown in half chambers) immediately after the onset of DDT for $d = 3$ mm and $d = 1.5$ mm with varying temperatures. The detonation wave is indicated by the red schlieren isolines near the localised regions marked as "DW". To demonstrate the stochasticity of DDT with varying temperatures and provide a global view of their localised regions, individual detonation waves under different initial conditions highlighted in Fig. 5 are projected onto a single main chamber shown in Fig. 6. It is observed in Fig. 5 that detonative regions for all tested cases are formed at the flame front when it propagates closely towards the wall. Then the regions grow significantly larger in a short period promoting the transition of the deflagrative flame to detonation. However, the DDT is found to be a stochastic process in the sense that the time and location for detonation onset are significantly different under the slightly different initial temperatures for certain orifice sizes. This is likely because the system in this study involves multiple stochastic phenomena, including turbulent flow instabilities, flame-shock interactions, complex shock wave distributions, etc.

In order to quantitatively demonstrate the stochasticity of DDT, Fig. 7 shows the time histories of the flame surface length

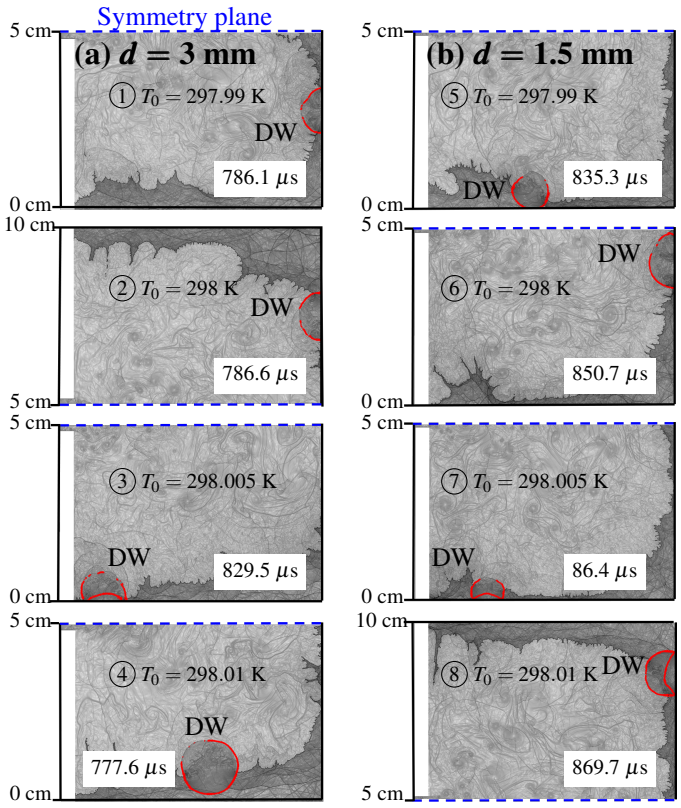


**FIGURE 5**: Distributions of schlieren fields for $d =$ left: (a) 3 mm and right: (b) 1.5 mm when $T_0 = 297.99$ K, 298 K, 298.005 K and 298.01 K. DW denotes the newly ignited detonation wave. The red contours are detonation waves defined by a schlieren isoline near the detonation regions. The blue dashed line indicates the symmetry plane.

and total heat release rate (HRR) for all tested cases. The total HRR is computed by averaging the HRR along the flame surface, and only the results within the period of the DDT process are shown in Fig. 7. For $d = 3$ mm, the flame surface length increases synchronously under all background temperatures before the flame front hits the orifice at about 0.29 ms. Then the development of the flame surface starts to slightly dissimilate among the different initial temperatures as the jet flame forms. Minimal differences are observed as the turbulent jet flame reaches a relatively "steady" state with fewer wrinkles in the main chamber and interacts with the reflected shock waves. Differences are found as the flames reach the end wall, where continuous flame-shock interactions are observed. The onset of detonation can be seen from the sharp increase of HRR as well as the sudden drop of flame surface length. The case with $T_0 = 298.005$ K is found to have a slightly delayed DDT compared to the cases with other initial temperatures. However, no significant differences are seen in all cases with the orifice size of $d = 3$ mm in terms of the flame surface length and total HRR.

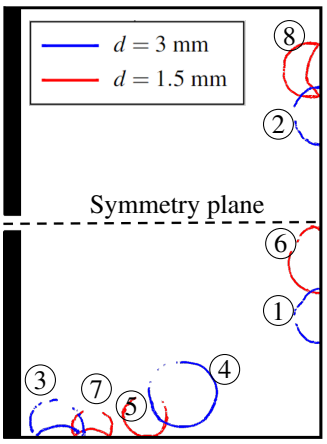


**FIGURE 6**: Stochastic nature of localised detonation waves for DDT. The blue and red contours are detonation waves defined by a schlieren isoline near the detonation initiation regions. The initial condition stamps for ①-⑧ are: ①: $d = 3$ mm, $T_0 = 297.99$ K, ②: $d = 3$ mm, $T_0 = 298$ K, ③: $d = 3$ mm, $T_0 = 298.005$ K, ④: $d = 3$ mm, $T_0 = 298.01$ K, ⑤: $d = 1.5$ mm, $T_0 = 297.99$ K, ⑥: $d = 1.5$ mm, $T_0 = 298$ K, ⑦: $d = 1.5$ mm, $T_0 = 298.005$ K, ⑧: $d = 1.5$ mm, $T_0 = 298.01$ K.

For $d = 1.5$ mm, the laminar flame and jet flame development are seen to have a slightly larger deviation compared to the ones seen in $d = 3$ mm. Furthermore, the second soar of the flame surface length when the flame and shocks continuously interact are found to be more distinctly different at the different initial temperatures for $d = 1.5$ mm, compared to their counterparts for $d = 3$ mm. This phenomenon indicates the formation of increasingly different turbulent flames under the four initial temperatures for $d = 1.5$ mm due to more different flame-shock interactions before the occurrence of DDT. Perhaps more interestingly, it is found that the maximum value of total HRR when DDT occurs reaches $1.51\times10^{10}$ W/m when $T_0 = 297.99$ K, almost twice larger than the total HRR of $6.99\times10^{9}$ W/m when $T_0 = 298.01$ K. The stochasticity behavior observed in $d = 1.5$ mm case can be related to the effect of orifice size where a small orifice is found to have delayed a detonation process where a prolonged flame-shock interaction period exists. As suggested by Oran and Gamezo [18] that high-Reynolds number flows are stochastic in a sense that they can be very sensitive to minimum changes in initial conditions, especially when DDT and flame-shock interactions are involved [18]. Therefore a delayed onset of DDT can be the possible reason for higher stochasticity, as seen in the case of $T_0 = 297.99$ K for $d = 1.5$ mm.

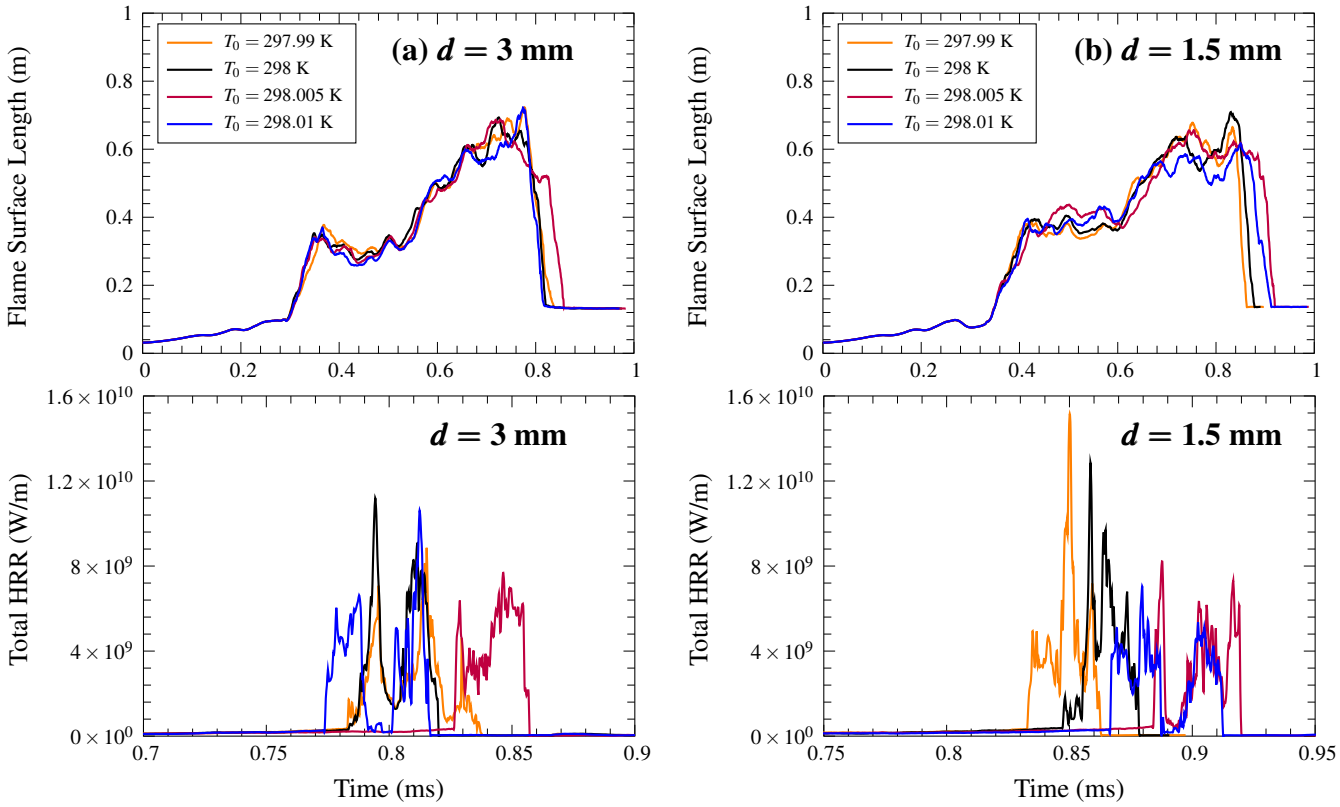


**FIGURE 7**: Time histories of computed flame surface length (top), and total heat release rate, i.e. HRR (bottom) for $d =$ left: (a) 3 mm and right: (b) 1.5 mm with a varying initial temperature.

In general, the stochastic behaviours of the temporal variations of the flame surface length and the total HRR are found during the processes of jet flame formation, flame-shock interactions, and DDT onset for both $d = 3$ mm and $d = 1.5$ mm based on the details discussed above. The configuration of the pre-chamber/main-chamber system with the smaller orifice size when $d = 1.5$ mm is found to be more sensitive to the stochasticity of DDT. Due to the physical complexity and the high costs of the simulations, how exactly such small-scale perturbations affect the large-scale behaviour of a system remains a question largely unaddressed in turbulent reacting flows. However, it is important to understand whether a particular DDT mechanism is, in fact, robust to small variations in a turbulent, stochastic flow.

### 3.2.3 Detonation Initiation Mechanism

In order to examine the DDT initiation mechanism, Fig. 8 depicts the enlarged schlieren fields around the localised explosive regions just after the detonation initiation for both $d =$ 3 mm and $d = 1.5$ mm when $T_0 = 297.99$ K and 298.01 K. In all of these simulations, the detonation is initiated at the tip of a finger flame when the flame front becomes very close to the bottom or end walls. Three main shocks (marked in Fig. 8) are observed by a strong schlieren gradient, and they collide at the flame front, causing the flame front to transition into a detonation. The possible underlying mechanism is that the shock focusing enhances the localised reactivity at the tip of the finger flame, thereby leading to its transition into detonation inside the flame brush. This shock-focusing mechanism is consistent with the results observed in DDT simulations in open obstructed channels by Xiao *et al.* [11] using one-step chemistry and by Dounia *et al.* [27] using detailed chemistry. As discussed previously, in all the cases presented in Fig. 8, the onset of detonation occurs at different times and locations. Despite this stochastic nature of DDT initiation, the shock-focusing mechanism is indeed found to be robust and insensitive to the small changes in initial temperature.

### 3.2.4 Effects of grid resolution

Additional resolution tests are performed to validate the

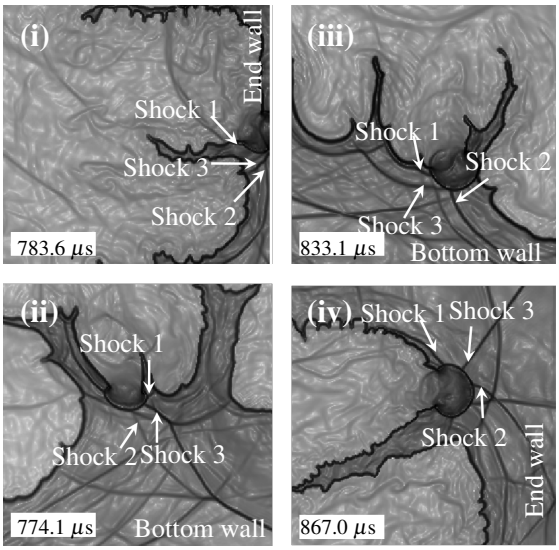


**FIGURE 8**: Schlieren fields showing shocks colliding at the flame tip to initiate detonation for (i) $d = 3$ mm, $T_0 = 297.99$ K, (ii) $d = 3$ mm, $T_0 = 298.01$ K, (iii) $d = 1.5$ mm, $T_0 = 297.99$ K, and (iv) $d = 1.5$ mm, $T_0 = 298.01$ K.

reliability of the numerical results. Numerical simulations have been performed with 2, 3, and 4 levels of refinement, corresponding to the minimum cell sizes of 13.0, 26.0, and 52.1 $\mu$m. Time histories of computed flame surface length using three different grid resolutions are shown in Fig. 9. For a finer grid, it takes a longer time for the flame to develop and eventually transit into a detonation. In general, the overall motions of the flame converge with the increasing grid resolution. However, the resolution test shows a divergent behavior near the detonation point (the sharp decrease of flame surface length). This is because the standard resolution tests have not taken into account the stochastic nature of turbulence and DDT in this system. Due to the limitation of computing resources, simulations with a finer grid size are impractical. On the other hand, a finer grid would also be unnecessary for the current study since the physics of interest are insensitive to grid resolutions. In this paper, simulations are performed with a 3 level of refinement, corresponding to a minimum cell size of 26.0 $\mu$m as a tradeoff between accuracy and computational cost.

## 4 Conclusions

Multidimensional, unsteady numerical simulations of an initially homogeneous mixture of stoichiometric ethylene-oxygen were performed to study the process of flame propagation and transition to detonation in a closed pre-chamber/main-chamber system. The simulations solved the fully compressible Navier-Stokes equations coupled with a

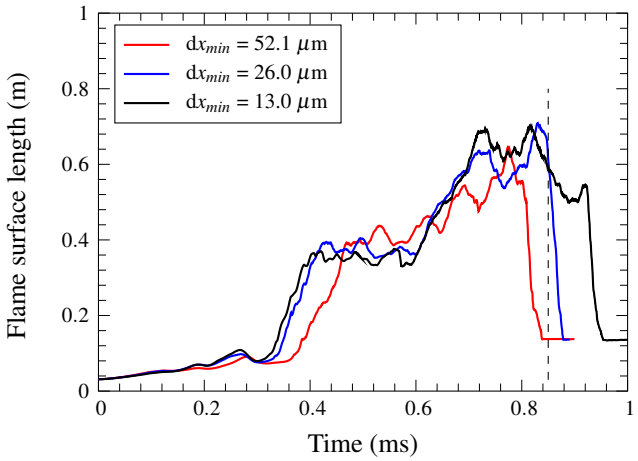


**FIGURE 9**: Time histories of computed flame surface length using three different grid resolution.

calibrated one-step chemical model. The overall process of DDT can be described in the following stages. First, a laminar flame propagates slowly in the pre-chamber. As the laminar flame hits the orifice, a turbulent jet flame is formed, inducing a strong leading shock wave in front of the jet flame. This leading shock wave propagates in the main chamber, bounces back from the end wall, and, in turn, interacts with the flame surface. The shock flame interaction induces flame instabilities that later develop into finger-shaped structures. Eventually, a detonation occurs at the flame tip as the turbulent flame almost fills up the chamber due to a shock-focusing mechanism.

To explore the effect of orifice size on DDT, simulation results with $d = 3$ mm and 1.5 mm are compared. While the main stages of the process remain qualitatively similar for both cases, there is an obvious delay for the case with a smaller orifice in terms of the flame propagation and transition to detonation. This apparent difference emerges as the flame passes through the orifice, forming a highly turbulent jet flame in the main chamber. The jet flame with $d = 1.5$ mm requires a longer time to develop compared to the case with $d = 3$ mm. In addition, the onset of DDT for the case with a smaller orifice size is also found to occur at a later time compared to the case with a larger orifice.

The stochastic nature of DDT and the sensitivity of the system to small changes in computational parameters are studied by varying the initial background temperature by a small amount. Simulations with an initial temperature of 297.99 K, 298 K, 298.005 K, and 298.01 K for both $d = 3$ mm and $d = 1.5$ mm are tested. It is found that under all of these conditions, the hot spot for detonation initiation is always generated at the tip of a finger flame near the walls. However, a stochastic distribution of the detonation initiation spots is observed for the cases with

varying initial temperatures. The configuration with a smaller orifice size ($d = 1.5$ mm) is more sensitive to changes in the initial temperature compared to that of $d = 3$ mm. Lastly, although the times and locations for detonation initiation are stochastic, all of the explosive kernels for the different orifice sizes and background temperatures are initiated by a shock-focusing mechanism, which is robust and insensitive to initial conditions changes and orifice sizes.

## ACKNOWLEDGMENT

This study was supported by the National Science Foundation of China (Grant No. 12002207). The work done at SJTU was supported by the school of aeronautics and astronautics, Shanghai Jiao Tong University. All the computations were carried out on SJTU supercomputing resources (https://hpc.sjtu.edu.cn/). Ruixuan Zhu acknowledges the financial support of Henry Lester Trust and China Oxford Scholarship Fund. Dr. XiaoHang Fang gratefully acknowledge the financial support from the John Fell Oxford University Press Research Fund. The authors are particularly grateful to Professor Elaine Oran for developing and sharing the computing code.

## REFERENCES

[1] Rapp, V., Killingsworth, N., Therkelsen, P., and Evans, R., 2016. "4 - lean-burn internal combustion engines". In *Lean Combustion (Second Edition)*, D. Dunn-Rankin and P. Therkelsen, eds., second edition ed. Academic Press, Boston, pp. 111–146.

[2] Alvarez, C. E. C., Couto, G. E., Roso, V. R., Thiriet, A. B., and Valle, R. M., 2018. "A review of prechamber ignition systems as lean combustion technology for si engines". *Applied Thermal Engineering,* ***128***, pp. 107–120.

[3] Wei, H., Gao, D., Zhou, L., Feng, D., and Chen, R., 2017. "Different combustion modes caused by flame-shock interactions in a confined chamber with a perforated plate". *Combustion and Flame,* ***178***, pp. 277–285.

[4] Zhao, J., Zhou, L., Zhong, L., Zhang, X., Pan, J., Chen, R., and Wei, H., 2019. "Experimental investigation of the stochastic nature of end-gas autoignition with detonation development in confined combustion chamber". *Combustion and Flame,* ***210***, pp. 324–338.

[5] Wang, Z., Liu, H., and Reitz, R. D., 2017. "Knocking combustion in spark-ignition engines". *Progress in Energy and Combustion Science,* ***61***, pp. 78–112.

[6] Qin, F., Shah, A., Huang, Z., Peng, L., Tunestal, P., and Bai, X., 2018. "Detailed numerical simulation of transient mixing and combustion of premixed methane/air mixtures in a pre-chamber/main-chamber system relevant to internal combustion engines". *Combustion and Flame,* ***188***, pp. 357–366.

[7] Merotto, L., Balmelli, M., Vera-Tudela, W., and Soltic, P., 2022. "Comparison of ignition and early flame propagation in methane/air mixtures using nanosecond repetitively pulsed discharge and inductive ignition in a pre-chamber setup under engine relevant conditions". *Combustion and Flame,* ***237***, p. 111851.

[8] Benekos, S., Frouzakis, C. E., Giannakopoulos, G. K., Bolla, M., Wright, Y. M., and Boulouchos, K., 2020. "Prechamber ignition: An exploratory 2-d dns study of the effects of initial temperature and main chamber composition". *Combustion and Flame,* ***215***, pp. 10–27.

[9] Wei, H., Zhao, J., Zhang, X., Pan, J., Hua, J., and Zhou, L., 2019. "Turbulent flame-shock interaction inducing end-gas autoignition in a confined space". *Combustion and Flame,* ***204***, pp. 137–141.

[10] Zhou, L., Li, K., Zhao, J., Zhang, X., and Wei, H., 2020. "Experimental observation of end-gas autoignition and developing detonation in a confined space using gasoline fuel". *Combustion and Flame,* ***222***, pp. 1–4.

[11] Xiao, H., and Oran, E. S., 2019. "Shock focusing and detonation initiation at a flame front". *Combustion and Flame,* ***203***, pp. 397–406.

[12] Zhu, R., Zhao, M., and Zhang, H., 2021. "Numerical simulation of flame acceleration and deflagration-to-detonation transition in ammonia-hydrogen/oxygen mixtures". *International Journal of Hydrogen Energy,* ***46***(1), pp. 1273–1287.

[13] Gamezo, V. N., Ogawa, T., and Oran, E. S., 2007. "Numerical simulations of flame propagation and ddt in obstructed channels filled with hydrogen-air mixture". *Proceedings of the Combustion Institute,* ***31***(2), pp. 2463–2471.

[14] Liberman, M., Ivanov, M., Kiverin, A., Kuznetsov, M., Chukalovsky, A., and Rakhimova, T., 2010. "Deflagration-to-detonation transition in highly reactive combustible mixtures". *Acta Astronautica,* ***67***(7), pp. 688–701.

[15] Gamezo, V. N., Ogawa, T., and Oran, E. S., 2008. "Flame acceleration and ddt in channels with obstacles: Effect of obstacle spacing". *Combustion and Flame,* ***155***(1), pp. 302–315.

[16] Oran, E. S., 2011. "Stochasticity and dynamics of high-speed reactive flows". *AIP Conference Proceedings,* ***1376***(1), pp. 38–44.

[17] Gamezo, V. N., Ogawa, T., and Oran, E. S., 2008. "Flame acceleration and ddt in channels with obstacles: Effect of obstacle spacing". *Combustion and Flame,* ***155***(1-2), pp. 302–315.

[18] Oran, E. S., and Gamezo, V. N., 2007. "Origins of the deflagration-to-detonation transition in gas-phase combustion". *Combustion and Flame,* ***148***(1), pp. 4–47.

[19] Toro, E. F., 2013. *Riemann solvers and numerical methods for fluid dynamics: a practical introduction*. Springer Science & Business Media.

[20] Houim, R. W., and Kuo, K. K., 2011. "A low-dissipation and time-accurate method for compressible multi-component flow with variable specific heat ratios". *Journal of Computational Physics,* ***230***(23), pp. 8527–8553.

[21] Fureby, C., and Moller, S. I., 1995. "Large eddy simulation of reacting flows applied to bluff body stabilized flames". *AIAA journal,* ***33***(12), pp. 2339–2347.

[22] Grinstein, F., Gutmark, E., Parr, T., Hanson-Parr, D., and Obeysekare, U., 1996. "Streamwise and spanwise vortex interaction in an axisymmetric jet. a computational and experimental study". *Physics of Fluids,* ***8***(6), pp. 1515–1524.

[23] Knight, D., Zhou, G., Okong'o, N., and Shukla, V., 1998. "Compressible large eddy simulation using unstructured grids". In 36th AIAA Aerospace Sciences Meeting and Exhibit, p. 535.

[24] Kessler, D., Gamezo, V., and Oran, E., 2010. "Simulations of flame acceleration and deflagration-to-detonation transitions in methane–air systems". *Combustion and Flame,* ***157***(11), pp. 2063–2077.

[25] Bell, J. Boxlib user's guide (2013). `https://ccse.lbl.gov/BoxLib/`.

[26] Zhou, L., Gao, D., Zhao, J., Wei, H., Zhang, X., Xu, Z., and Chen, R., 2018. "Turbulent flame propagation with pressure oscillation in the end gas region of confined combustion chamber equipped with different perforated plates". *Combustion and Flame,* ***191***, pp. 453–467.

[27] Dounia, O., Vermorel, O., Misdariis, A., and Poinsot, T., 2019. "Influence of kinetics on ddt simulations". *Combustion and Flame,* ***200***, pp. 1–14.